Construction and Building Materials 394 (2023) 132261

Contents lists available at ScienceDirect

Construction and Building Materials

journal homepage: www.elsevier.com/locate/conbuildmat

Crystallisation and phase transformation processes during clinkering in portland cement (pc) by means of in situ and ex situ analyses

M. Cantaluppi [a,*], V. Diella [b], A. Pavese [c], M. Marchi [d], N. Marinoni [a]

[a] Earth Sciences "Ardito Desio" Department, Università degli Studi di Milano, Via S. Botticelli 23, 20133 Milano, Italy
[b] Consiglio Nazionale delle Ricerche, IGAG, Sezione di Milano, Via S. Botticelli 23, 20133 Milano, Italy
[c] Earth Sciences Department, Università degli Studi di Torino, Via Valperga Caluso 35, 10123 Torino, Italy
[d] Global Product Innovation (GPI) Department, Italcementi S.p.A., Heidelbergcement Group, Bergamo, Italy

ARTICLE INFO

Keywords:
Ordinary portland cement
Doped clinker
X-ray powder diffraction
Synchrotron diffraction
Rietveld quantitative phase analysis
Waste reuse

ABSTRACT

An important challenge of cement industry is the waste reuse as a feasible substitute of natural materials, thus reducing cement manufacture footprint. A critical gap in literature is the lack of a comprehensive overview on minor element effects commonly carried from wastes. This study aimed to fill this gap investigating the effects of multiple minor element occurrence (Mg, S, Na and Cl) on Ordinary Portland Clinker mineralogy, microstructure, phase polymorphism and chemical reactions occurring during clinkering. The findings highlighted that minor elements are strongly correlated to each other in influencing clinker properties: during clinkering, all raw meals exhibited similar reaction temperatures and melting phase formation; conversely, large differences are observed on reactivity, crystal phase composition and polymorphism.

1. Introduction

Concrete is the most widely used construction material owing to its excellent mechanical and durability properties. Nearly one ton of concrete is produced for every human being in the world each year [1], leading to ten billion tons of concrete annually. Its production is totally dependent on primary raw materials, such as limestone, clay minerals and/or marls mixed in appropriate proportions. Reducing the environmental impact of the concrete production is a crucial target for global sustainability and can be pursued by exploitation of waste materials in replacement of the natural ones, in building industry.

Nowadays, the use of recycled materials is one of the seven principles of sustainable construction and the past decade has seen an increasing application of wastes for application in cement, including industrial byproducts, such as fly ashes and bottom ashes, silica fume and blast furnace slags, gypsum, waste glasses and mine tailings.

Wastes have a large variability in terms of mineralogical and chemical composition and can have important effects on the final cement's phase assemblage and technical performance [2–4]. In a recent study [5], a multidisciplinary approach was developed to investigate the impact of the simultaneous occurrence of SO_3, MgO, Na_2O that are considered as the most frequently occurring minor components in industrial clinkers for Portland Cement (PC), giving cements that exhibit different behaviors upon hydration.

In the abovementioned paper, *in-situ* high-temperature X-Ray Powder Diffraction (XRPD) experiments, performed by a laboratory diffractometer, allowed us to clarify the clinkering reactions that take place upon heating, paying attention to: (i) chemical reaction rate; (ii) polymorphic transformations; (iii) liquid phase formation. Although the obtained results exhibit good accuracy for quantitative analyses, an approach using synchrotron radiation (SR) makes it possible to overcome most of the drawbacks in XRPD laboratory for *in-situ* experiments in cements, such as poor sample averaging, absorption effects or preferred orientation. The exceptional speed of data collection using SR allowed studies to get insight into hydration reactions of cement pastes [6]. Furthermore, the Synchrotron X-Ray Powder Diffraction (SXRPD) at non-ambient condition has already been used to characterize cements at high-temperature, hereafter reported as High-temperature Synchrotron X-Ray Powder Diffraction (HT-SXRPD). The main objectives are twofold: on the one hand, characterization of decomposition and formation products in cements systems and, on the other hand, investigation of the reactions taking place in the clinkering process at higher temperature. Few studies on cements have been reported in literature by HT-SXRPD, owing to the experimental complexity: an example is provided by De la Torre et al., [7,8], in which the clinkering reactions of active belite clinkers were followed by HT-SXRPD, to understand the

* Corresponding author.
E-mail address: marco.cantaluppi@unimi.it (M. Cantaluppi).

https://doi.org/10.1016/j.conbuildmat.2023.132261
Received 1 June 2022; Received in revised form 5 June 2023; Accepted 21 June 2023

role of borax, as an activating agent of Fe-rich belite sulpho-aluminate cements (BCSA).

The present work aims to complement the investigation of Segata et al. [5], so as to understand the impact of more complex combinations of minor elements on PC clinker. In particular, $CaCl_2$ was added to SO_3-MgO-Na_2O-doped industrial PC clinker kiln feeds and the induced effects on the clinkering process were studied. The reason why we chose of introducing chlorine in the mixture investigated by Segata et al. [5] is due to the fact that such a species is widespread in wastes, even though its behavior is almost unexplored. Cl occurs in organic (PVC, EPI, DMC, TCE and phosgene) and inorganic substances, and its content is a quality parameter that must be considered as it hardly affects both clinkering in kiln and technological performance of the final cement (i.e., mechanical resistance). Gerassimidou et al. [9] reports that, during combustion, most Cl remains within the kiln system causing operating problems and only a small percentage (0.7–1.3%) is incorporated into clinker, making it "stickier". Simoni et al. [10] recently explored the system CaO-SiO_2-Al_2O_3-SO_3-$CaCl_2$-MgO during clinkering, maintaining that in high concentration Cl is progressively incorporated into the C_3S crystals and Al-bearing phases that result from the alinite and/or chlormayenite formation, respectively. Yet, no studies have been published to date on Cl effects in combination with other common minor elements, during clinker production.

2. Sample preparation

Raw meals were prepared starting from an industrial raw mixture to reproduce the chemical composition of the PC clinker that represents the reference raw meal (*MIX_00,* Table 1). Certified chemical reagents (Carlo Erba Reagents), i.e., Na_2CO_3 (>99.5 wt%), $MgCO_3$ (>99.0 wt%), $CaSO_4{\cdot}2H_20$ (>99.0 wt%) and $CaCl_2$ (>99.5 wt%), were used as minor elements carriers for doped raw meals.

Fifteen doped raw meals were prepared by adding minor elements compounds to the *MIX_00* (Table 1): first, three raw meals were prepared to study the effects of magnesium, sulphur and sodium in coupled presence (*MIX_MN*, *MIX_NS*, *MIX_MS*); starting from these, twelve more raw mixes were prepared to study the role of different amounts of chlorine by adding $CaCl_2$ at 0.5, 1.0 and 1.5 wt%. The samples were labelled as *MIX_XXC0.5*, *MIX_XXC1*.0 and *MIX_XXC1.5* where *XX*: *00*, *MN*, *NS* and *MS*.

The raw meals were homogenized in an automatic shaker for 120 min and calcined in a furnace (Carbolite RHF 16/35 with SiC resistors) at 950 °C for 45 min to avoid carbon dioxide release during the firing cycle for both *ex-situ* and *in-situ* experiments [11]. After the calcination process, raw meals doped with chlorine were analysed by photometric titrations, to verify that no volatilization occurred.

Table 1
Chemical composition (wt.%) of raw meals prepared, as determined by XRF analysis; esd below 0.1 wt%.

Mix/Oxide	*MIX_00*	*MIX_MN*	*MIX_NS*	*MIX_MS*
CaO	42.30	40.83	41.87	40.86
SiO_2	13.63	13.16	13.48	13.15
Al_2O_3	3.25	3.14	3.22	3.14
Fe_2O_3	1.93	1.87	1.91	1.87
MgO	0.64	2.03	0.65	2.04
SO_3	0.20	0.21	0.91	0.92
Na_2O	0.09	0.42	0.41	0.10
K_2O	0.59	0.56	0.58	0.56
TiO_2	0.19	0.18	0.19	0.18
P_2O_5	0.09	0.09	0.09	0.09
Mn_2O_3	0.09	0.09	0.09	0.09
F	0.01	0.01	0.01	0.01
Cl	0.01	0.01	0.01	0.01
LOI	35.87	36.38	35.35	35.81
TOTAL	98.90	98.94	98.75	98.79

3. Experimental

3.1. X-Ray fluorescence (XRF)

The chemical composition of the starting raw meals was measured by XRF using a Bruker S8 Tiger WDXRF spectrometer with a Rh X-ray tube operating at 50 kV. The measurements were carried out on fused glass discs prepared by mixing 0.875 g of powdered whole samples with 6.125 g of lithium tetraborate lithium (corresponding to a 1:7 sample/borate dilution), carefully homogenized in a Pt (95%)-Au (3%)-Rh (2%) crucible and heated for 20 min at 1000 °C. Fusion of the flux reagent and sample was performed on a Pt-Au-Rh crucible using a CLAISSE FLUXER-BIS! automatic apparatus. Once the fusion was completed, the resulting melt was poured in a Pt-deep plate and slowly cooled [12].

3.2. Ex-situ laboratory X-Ray Powder Diffraction (LXRPD)

Ex-situ Laboratory X-Ray Powder Diffraction (LXRPD) were performed only on samples either without chlorine or with 1.0 wt% of $CaCl_2$. LXRPD data acquisition was carried out by a X'Pert PRO Diffractometer (PANalytical), in *θ-2θ* Bragg-Brentano geometry with diverging beam diffractometer, equipped with an X'Celerator LPS detector. The 1.23–7.75 *d* (Å) range has been investigated using CuKα radiation for all samples. LXRPD data collections were performed with 40 kV current tension, 40 mA current intensity, 0.02° step size, 120 s/step equivalent counting time and fixed divergence slits angle at 0.5°. Samples analysed with LXRPD were firstly grinded and then pressed in back-load sample holders.

3.3. In-situ High-temperature Synchrotron X-Ray Powder Diffraction (HT-SXRPD)

In-situ HT-SXRPD experiments were performed at ID22 (former ID31) beamline at the European Synchrotron Radiation Facility (ESRF) in Grenoble, France [13,14]. The diffractometer operates in Debye-Scherrer configuration with a wavelength of $\lambda = 0.32635$ Å, selected by a double-crystal Si (1 1 1) monochromator, minimizing the absorption effects due to the platinum capillary. The data from the monochromator Multi-Analyser Si (1 1 1) Stage coupled with the nine scintillation detectors were normalized and summed to 0.002° step size using local software to produce the final raw data. The 18–0.78 *d* (Å) range was explored.

A parabolic mirror furnace, equipped with three halogen lamps, was used to heat the Pt capillaries samples between 900 °C and 1450 °C [15]. The maximum efficiency of the furnace was achieved by constraining the lamps filaments in the same plane of the sample rotation axis and focusing a 4 mm section along this axis. A delay time of 5 min was set before collecting data at a given temperature, for thermal equilibration to be achieved. A variable voltage applied to the halogen lamps allowed control of temperature. The actual temperatures at the sample were obtained from the analysis of the Pt peak diffraction positions [16].

3.4. Rietveld quantitative phase analysis (RQPA)

LXRPD and SXRPD experimental profiles were fitted using the GSAS-ii software [17]. Instrumental calibration for both Synchrotron and Laboratory diffractometers was performed using LaB_6 (Standard NIST, SRM 660c) in the same experimental setups.

During Rietveld Quantitative Phase Analysis (RQPA), cell parameters, crystallite size, individual scale factor, zero shift and a Chebyshev polynomial function used to model the background, were refined [18,19].

The structure models of M_3-C_3S [20], M_1-C_3S [21,22], α'_H-C_2S and α'_L-C_2S [23], β-C_2S [24], cubic C_3A [25], orthorhombic C_3A [26], C_4AF [27], CaO [28], MgO [29], β-SiO_2 [30], $C_{12}A_7$ [31] and aphthitalite [32] were used for Rietveld analysis of *ex-situ* patterns. The structure models

of R-C_3S [33], high-temperature C_2S polymorphs for α, α'$_L$, α'$_H$ at 1545, 1060 and 1250 °C, respectively [23] were used for *in-situ* patterns. The room-temperature structure models for the remaining crystal phases, such as cubic and orthorhombic C_3A, C_4AF, $C_{12}A_7$ and CaO, were employed for high-temperature data treatment too, save that an overall isotropic thermal parameter was used, as large as 0.03 Å^2 [11].

3.5. Electron microprobe analysis (EMPA) and scanning electron microprobe (SEM)

Pellets of six chlorine doped samples *MIX_00C1.0, MIX_MNC1.0, MIX_NSC1.0, MIX_MSC1.0* fired at 1450 °C and two capillaries*, Raw meal 1_C1.5* and *Raw meal 2_C1.5* analyzed by HT-SXRPD were embedded in epoxide resin. Dry-out polishing conditions were applied using abrasive papers with decreasing grain size and finished with diamond paste (1 μm). An ultrasonic bath in hexane allowed removal of the residual powder from previous polishing. Samples were covered with a carbon layer to ensure conductivity. Backscattered electron images, used for microstructural analysis, and quantitative chemical analyses were performed using a JEOL JXA-8200 Electron MicroProbe Analyser in Wavelength-Dispersive mode (EMPA_WDS) at the laboratory of the Earth Sciences Department "Ardito Desio" of the University of Milan, with an accelerating voltage of 15 kV, a spot size of 1 μm, a beam current of 10nA, a counting times of 30 s on peaks and 10 s on backgrounds. The following elements were measured: Si, Ti, Al, Ca, Fe, K, Mg, Na, Mn, Sr, S, F and Cl. Natural minerals were used as standards and raw data were corrected for matrix effects using a conventional ΦρZ routine in the JEOL software package.

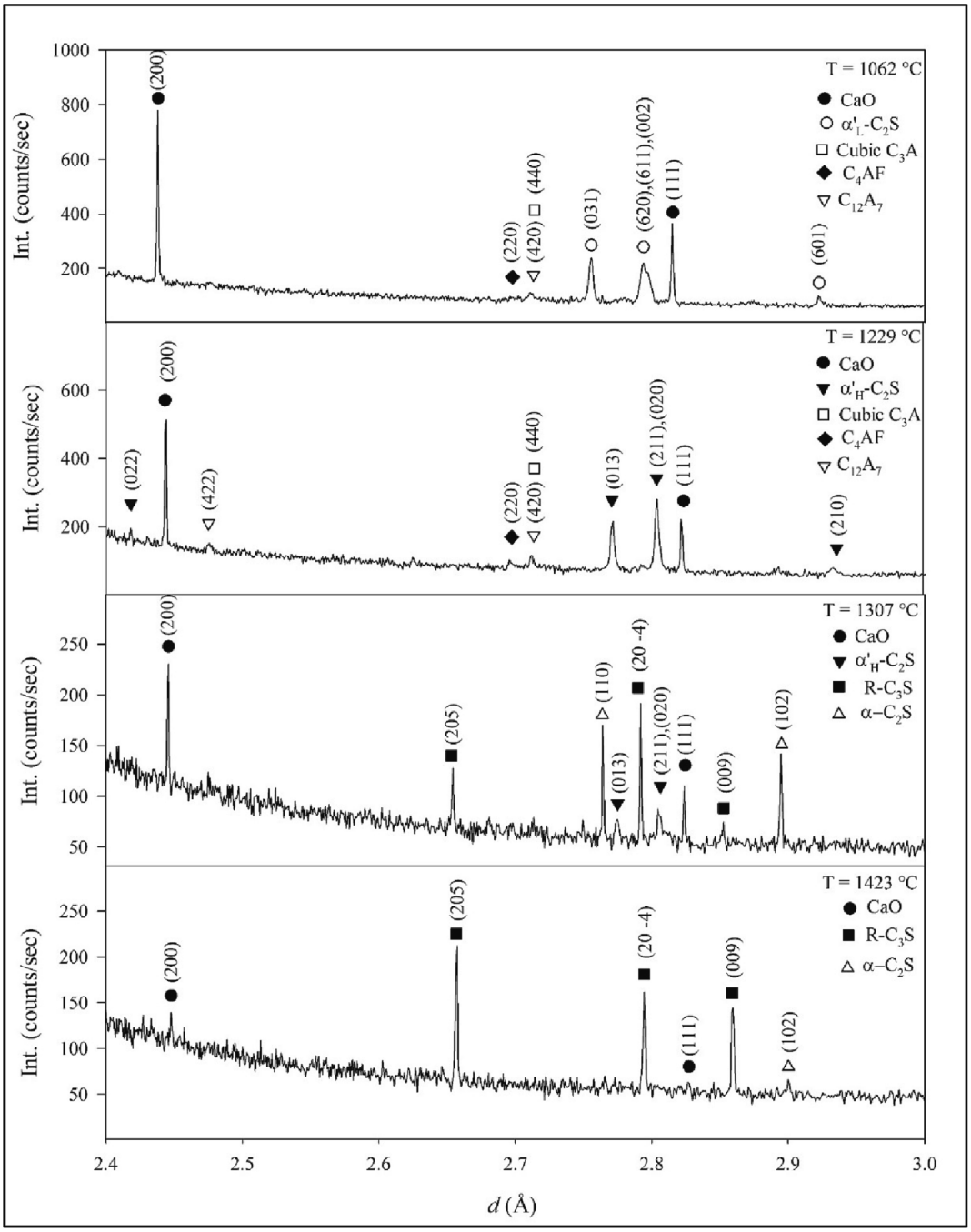

Fig. 1. In-situ HT-SXRPD patterns for MIX_MSC1.0 collected from 1062 to 1423 °C with main Bragg peaks labelled and indexed.

4. Results

4.1. In-situ high-temperature synchrotron X-ray powder diffraction (in-situ HT-SXRPD)

In-situ high-temperature patterns allow us to get insight into the main reactions taking place during heating. By way of example, Fig. 1 shows a selected range of SXRPD patterns collected during *in-situ* high-temperature experiments for *MIX_MSC1.0*. The results of the Rietveld analysis on four samples are displayed in Fig. 2 and show the effects of the dopants on the main phase contents as a function of temperature. Fig. 3 provides an example of the Rietveld fit agreement, for *MIX_MSC1.0* at 1062 °C.

An inspection of Fig. 2 suggests splitting the clinkering reaction into two stages: a *1st stage* at T < 1250 °C, approximately, where the chemical reactions take place at solid state without the occurrence of liquid phase; a *2nd stage* at T > 1250 °C, approximately, where the chemical reactions occur in presence of a liquid phase (clinkering zone) that is mainly composed of melted aluminate phases (C_3A, C_4AF and $C_{12}A_7$). In particular: (i) in the *1st stage*, all samples contain α'$_L$-C_2S, CaO, β-SiO_2, cubic C_3A and C_4AF, and no Bragg peaks of minor element carriers (sodium carbonate, periclase, anhydrite, calcium chlorine) were observed. Therefore, all minor elements are assumed to be hosted by the formed crystal phases or may contribute to give a separated liquid phase. Only β-SiO_2 was found also at *T* > 870 °C, in terms of tridymite occurrence. $C_{12}A_7$ occurs in all samples with 1.5 wt% of $CaCl_2$, also in *MIX_MN* and *MIX_MS* at 0.5 and 1.0 wt% doping values. No orthorhombic C_3A was found in any samples, even in sodium-rich samples. At *T* > 1100 °C, the polymorphic transition from α'$_L$-C_2S to α'$_H$-C_2S takes place and in none of the samples the co-existence of these two C_2S polymorphs was detected; (ii) in the *2nd stage*, all samples reveal a reduction of CaO and C_2S, due to crystallization of R-C_3S.

On the other hand, large differences among samples are observable in terms of phase proportions. In Table 2, the amounts of C_2S, C_3S and CaO at 1100 °C (solid state stage) and liquid phase at 1350 °C for all raw meals under investigation are reported for comparison. Furthermore, a Confidence Level was calculated by summing the overlapping Gaussian distribution area of the selected value and the reference one (*MIX_00*) (Fig. 1S in Supplementary Material).

The attention is focussed on four important aspects:

1) samples bearing two minor elements (*MIX_MN*, *_NS* and *_MS*) promote C_2S formation during the *1st stage* with respect to the reference samples (*MIX_00*), especially in the case of sodium-rich mixtures, yielding a decrease in CaO and SiO_2. For instance, at 1100 °C the C_2S amount in *MIX_MN* is ~ 63 wt% whereas in *_00* is ~ 55 wt%. On the contrary, at higher *T* (*2nd stage*), lower contents of C_2S are observed in doped samples, save for *MIX_NS* whose content remains constant throughout the heating process (45 wt% at 1450 °C);
2) no temperature differences were observed among samples in terms of first occurrence of C_3S. At temperature higher than 1250 °C, only magnesium-rich samples have an increase in C_3S content with respect to *MIX_00*. Conversely, *MIX_NS* has the lowest value of C_3S and the highest C_2S content (39.2 and 44.8 wt%, respectively) at 1350 °C;

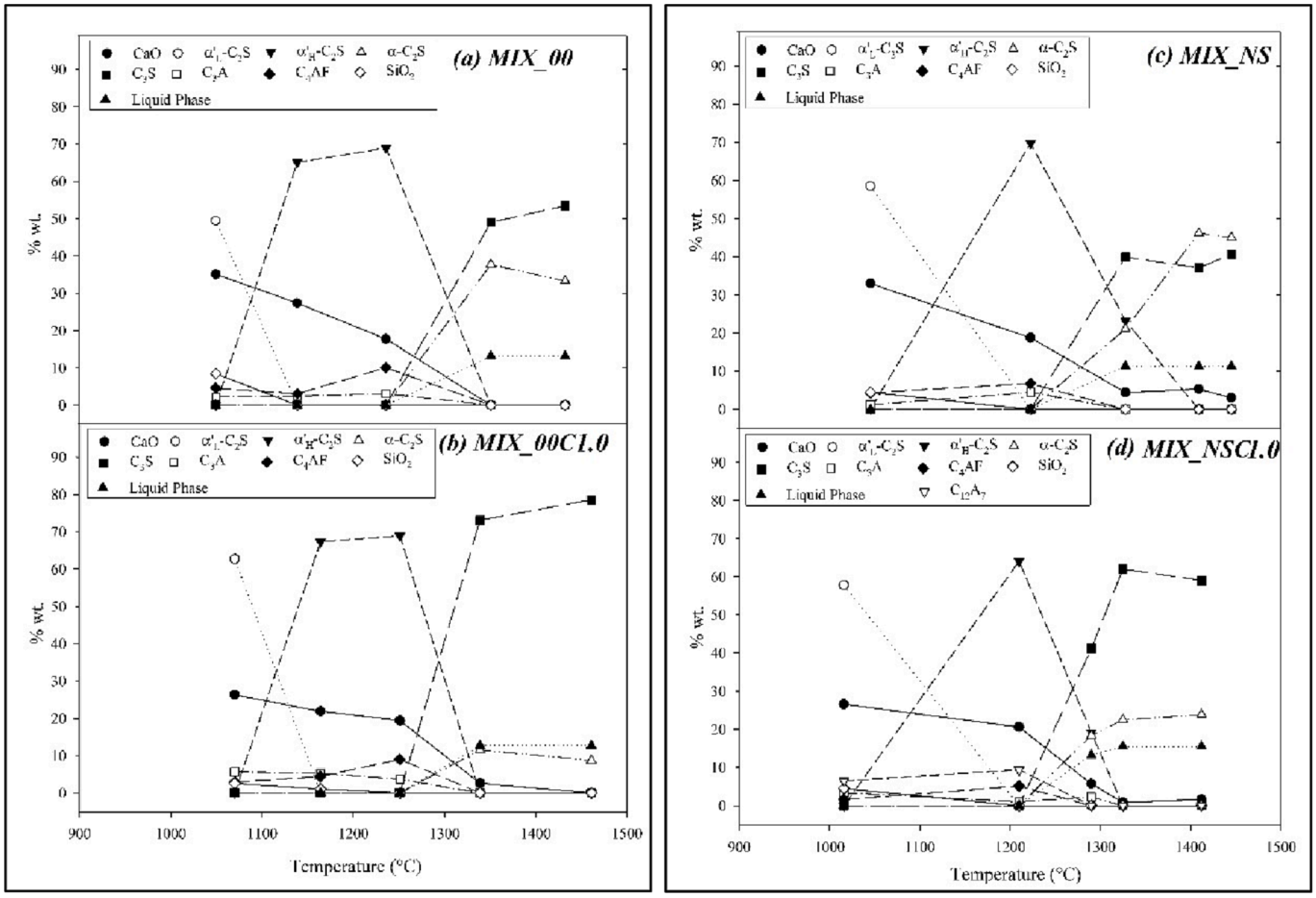

Fig. 2. In-situ HT-SXRPD results (wt.%) from Rietveld quantitative phase analysis vs temperature (°C) on heating for (a) MIX_00, (b) MIX_00C1.0, (c) MIX_NS and (d) MIX_NSC1.0; symbol size is always>3σ of all analyses.

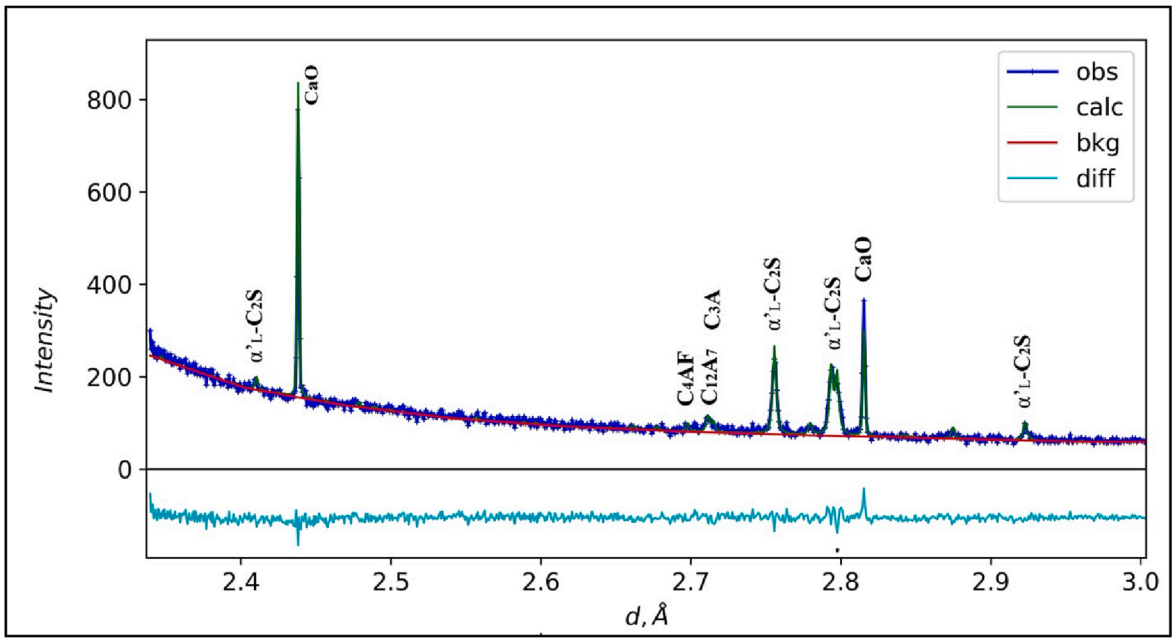

Fig. 3. Rietveld plot for MIX_MSC1.0 collected by means of in-situ HT-SXRPD at 1062 °C; main peaks are labelled.

3) at clinkering temperature (~1450 °C) all doped mixtures give higher CaO contents (~5 wt%) than *MIX_00*;
4) the liquid phase exhibits the lowest and highest amount for *MIX_MN* (8.1 wt%) and *MIX_MNC1.5* (19.4 wt%) respectively, whilst the other doped mixtures share figures comparable to that of *MIX_00*, within the range 11–16 wt%.

Comparing all chlorine-rich samples (*MIX_XXCX.X*) with those without chlorine (*MIX_XX*), three aspects are worth being stressed (Fig. 4):

1) during the *1st stage*, all chlorine-rich mixtures have lower CaO content than their counterparts without chlorine. C_2S has generally higher contents at 0.5 and 1.0 wt% of $CaCl_2$ doping, save for 1.5 wt% $CaCl_2$ samples, in which C_2S is similar to the mixture without chlorine addition;
2) during the *2nd stage*, all samples, except for all chlorine-doped *MIX_MN*, show an increase of C_3S and a decrease of C_2S content. Chlorine-doped *MIX_MN* mixtures reveal an increase of C_2S and a decrease of C_3S;
3) all chlorine-bearing mixtures (*MIX_XXCX.X*) show an increase of the liquid phase, related to the increased amount of aluminium-rich phases during the *1st stage* (C_3A, $C_{12}A_7$ and C_4AF), excepted for *MIX_00CX.X* mixtures that do not show any remarkable change as confirmed by the high values of Confidence Level (Table 2).

No robust linear relationship can be established between $CaCl_2$ content and clinker phases (i.e., C_2S and C_3S amounts).

Considering the normalized volume (V/Z; $Å^3$) *versus* temperature trend on heating for the main crystal phases, four important features can be highlighted:

1) in any investigated sample no remarkable volume cell changes *versus* temperature occur for α'_L-C_2S and α'_H-C_2S. Lower cell volume values are observed for α-C_2S in *MIX_MN* on the explored *T* range. Moreover, α-C_2S has larger cell volume for all chlorine-rich samples in comparison with the same mix without chlorine (in Fig. 5, the results for all samples without and with 1 wt% of $CaCl_2$ are reported; in Fig. 2S the results only for α-C_2S are reported);
2) R-C_3S cell volume (Fig. 3S) shows lower values for all magnesium-rich samples, especially for *MIX_MN*, while higher values occur for *MIX_NSC1.0* and *MIX_00C1.0*. All chlorine-rich mixtures have larger cell volume values than those in the same mixtures without chlorine addition, save for *MIX_MS*. These features are more pronounced during the late *2nd stage* with respect to the first one;
3) the cubic C_3A cell volume changes (Fig. 4S) over a wide range of value during the early *1st stage* (<1100 °C), with larger values for all chlorine-rich samples and a very slowly increasing trend *versus* temperature. During middle and late *1st stage* (1100 – 1200 °C), cell volume changes are smaller between all samples, but sulphur-rich and chlorine-rich mixtures have higher values with respect to *MIX_00* and *MIX_MN*;
4) C_4AF cell volume has higher values (Fig. 5S) for all chlorine-rich mixtures in comparison with the same samples without chlorine; in addition, during early *1st stage* very large cell volume values are observed for mixtures doped with both chlorine and sulphur.

4.2. *Ex-situ laboratory X-ray Powder Diffraction (LXRPD)*

Considering *ex-situ* LXRPD Rietveld results (Table 1S, Fig. 6, Fig. 7) for samples doped only with sulphur, magnesium and sodium, three main points are stressed:

1) all samples share similar contents of C_3S + C_2S wt.%, though with different C_3S/C_2S ratios and nature of the occurring polymorphs. *MIX_MN* has a strong increase of C_3S/C_2S, with a preferred stabilization of M_3-C_3S and α'_H-C_2S; whereas *MIX_NS* and *MIX_MS* show a decrease of M_3-C_3S, and β-C_2S, only, is observed in *MIX_MS*;
2) the amount of C_3A + C_4AF is similar for all mixtures, save for *MIX_MN* that reveals a sharp increase due to C_3A. All samples doped with sodium have an increase in C_3A, and the orthorhombic polymorph is preferred if sulphur is absent (*MIX_MN*). *MIX_MS* show a strong increase of C_4AF/C_3A and only cubic C_3A occurs;
3) periclase occurs only if magnesium is introduced in the raw meal; CaO appears in all mixtures in similar figures, but for *MIX_NS* that exhibits a double amount.

Considering *ex-situ* LXRPD Rietveld results of chlorine-rich samples (*MIX_XX_C1.0*) and comparing them with the corresponding mixtures

Table 2
In-situ HT-SXRPD results for C_2S, C_3S and CaO during solid state stage at 1100 °C and liquid phase stage at 1350 °C for all raw meals; esd (3σ) is reported within round brackets and was obtained from the RQPA by mean of GSAS-ii software [17]; * Within square brackets is reported the Confidence Level which was calculated by summing the percentage of overlap of Gaussian distribution of target range and reference range of MIX_00 (see Fig. 1S).

	Solid statereaction region wt.% at 1100 °C		Liquid phase reaction region wt.% at 1350 °C			
Sample	C_2S	CaO	C_2S	CaO	C_3S	Liquid phase
MIX_00	54.6 (1.6) [*Ref.*]*	30.5 (4) [*Ref.*]	38.1 (1.1) [*Ref.*]	0.2(8) [*Ref.*]	48.5 (1.7) [*Ref.*]	13.2 (1.4) [*Ref.*]
MIX_00C0.5	57.0 (1.4) [7%]	27.7 (7) [-]	11.5 (1.3) [-]	10.4(9) [-]	63.6 (1.6) [-]	14.5 (1.4) [117%]
MIX_00C1.0	63.7 (1.3) [-]	25.2 (5) [-]	11.3 (1.5) [-]	2.3(3) [-]	73.7 (1.6) [-]	12.7 (1.3) [194%]
MIX_00C1.5	53.7 (1.1) [162%]	20.3 (6) [-]	17.8 (1.2) [-]	3.1(5) [-]	61.3 (1.2) [-]	14.2 (1.2) [151%]
MIX_MN	62.7 (1.6) [-]	28.2 (0.5) [-]	11.0 (1.3) [-]	5.9(5) [-]	75.0 (1.4) [-]	8.1(9) [-]
MIX_MNC0.5	64.0 (1.3) [-]	26.1 (3) [-]	14.8 (1.3) [-]	3.5(6) [-]	63.9 (1.2) [-]	10.5(6) [-]
MIX_MNC1.0	64.1 (1.7) [-]	26.3 (4) [-]	16.1 (1.1) [-]	1.1(3) [125%]	72.4 (9) [-]	10.4(9) [-]
MIX_MNC1.5	59.0 (1.8) [-]	24.3 (5) [-]	12.5 (1.2) [-]	5.3(5) [-]	61.4 (8) [-]	19.4 (1.2) [-]
MIX_NS	61.9 (1.4) [-]	28.7 (6) [-]	44.8 (1.4) [-]	4.7(7) [-]	39.2 (1.4) [-]	11.3 (1.6) [43%]
MIX_NSC0.5	63.8 (1.2) [-]	23.3 (7) [-]	21.0 (7) [-]	0.4(4) [200%]	65.3 (1.3) [-]	11.3 (1.2) [17%]
MIX_NSC1.0	60.5(8) [-]	24.0 (3) [-]	22.4 (6) [-]	1.1(2) [72%]	61.0 (1.0) [-]	15.5 (1.2) [2%]
MIX_NSC1.5	63.8 (0.6) [-]	25.2 (0.4) [-]	10.4 (5) [-]	3.6(7) [-]	70.9 (1.3) [-]	15.1 (1.2) [17%]
MIX_MS	58.4 (1.5) [-]	28.0 (0.6) [-]	24.1 (1.1) [-]	5.9(6) [-]	56.1 (2.0) [-]	13.9 (1.5) [188%]
MIX_MSC0.5	65.8 (1.3) [-]	17.1 (0.4) [-]	16.6 (1.2) [-]	0.6(3) [200%]	65.7 (1.7) [-]	14.2 (1.3) [156%]
MIX_MSC1.0	61.2 (1.3) [-]	23.8 (0.5) [-]	16.5 (1.1) [-]	7.2(7) [-]	59.5 (2.3) [-]	16.8 (1.9) [-]
MIX_MSC1.5	59.5 (1.2) [-]	22.9 (4) [-]	13.7 (1.0) [-]	4.6(4) [-]	65.2 (2.0) [-]	16.4 (1.7) [-]

without chlorine addition (*MIX_XX*), three main points are underscored:

1) a decrease of C_3S content occurs for all samples, but for *MIX_00C1.0*, along with the C_3S M_3/M_1 ratio, especially in samples doped with sulphur (Fig. 6);
2) an increase of C_2S occurs in chlorine-rich samples, due to β-C_2S (Fig. 6);
3) C_3A content had a marked decrease, and the cubic polymorph was preferred stabilized, whereas C_4AF increased except for *MIX_MSC1.0* (Fig. 6).

Furthermore, a Confidence Level was calculated (as for *in-situ* Results, Table 2) for C_3S and C_2S using *MIX_00* as referee (Table 1S in Supplementary Material): C_3S wt.% was similar in all doped mixtures except for *MIX_MN*, *MIX_NSC1.0* and *MIX_MSC1.0*; whereas only C_2S wt.% in *MIX_NSC1.0* was similar to *MIX_00*.

The effect of dopants on the normalized volume (volume of formula unit, V/Z, Å^3 [34]) for both M_1-C_3S and M_3-C_3S are reported in Fig. 8. Magnesium produced a clear volume decrease, whereas sulphur caused the opposite effect. Adding chlorine slightly increases the cell volume of tricalcium silicate, without any preferences between M_1 and M_3 polymorphs.

Considering the obtained normalized volumes (V/Z, Å^3) for β-C_2S for all samples (Fig. 9) reveals that sulphur is responsible of the cell volume increase, whereas magnesium produces no significant change. Chlorine strongly increases the cell volume for all samples.

As for aluminates, the normalized volume (V/Z, Å^3) of cubic C_3A (Fig. 9S) decreases for sulphur-rich and chlorine-rich, save for *MIX_NSC1.0* where the normalized volume remains almost unchanged. For C_4AF (Fig. 10S), sodium-rich and sulphur-rich (*MIX_MN,NS,MS*) mixtures produced a slight volume increase and decrease respectively, whereas the chlorine-rich mixtures (*MIX_XX_C1.0*) gave a decrease in cell volume, especially in presence of sodium (*MIX_MN,NS_C1.0*).

4.3. Microprobe and scanning electron microscopy analyses

In Table 3 the average analyses of the main phases in the clinker sampled doped with 1.0 and 1.5 wt% $CaCl_2$ are shown. No differences in the chemical composition of the calcium silicate crystals in terms of major oxide are observed, as with aluminate. Differences are found in minor elements contents as a function of the added doping elements in the raw meals: MgO is preferentially incorporated in the C_3S structure, even if Mg-rich C_4AF is observed. Analyses of Na-enriched clinkers reveal high sodium oxide content of ~ 0.5–0.6 wt% in the C_2S crystals. In the S-doped clinkers a preference of sulphur for C_2S and C_4AF crystals is observed. Note that ferrite crystals exhibited high contents of dopants in all the studied samples.

Finally, little amounts of chlorine are detected in ferrite crystals within *MIX_00C1.5* and *MIX_MSC1.0* only.

All BSE images show similar microstructural features of clinker among samples: alite occurs as prismatic, pseudohexagonal crystal shape, commonly larger than belite crystals; belite appears as rounded and extremely fractured crystals both in cluster and inside alite crystals; the interstitial phase occurred as a thin micrometric ferrite and celite intergrowth (Figs. 10, 11).

Microprobe analyses prove occurrence of a strong Cl volatilization in all mixtures during thermal treatment, independently of the minor element combination. A small amount of chlorine is present in ferrite analyses of alkali-free clinkers *MIX_00C1.0* and *MIX_MSC1.0*.

SEM investigation of cross-sections of the two capillaries containing clinker obtained from thermally treating of raw meal doped with $CaCl_2$ addition, revealed a significant volumetric shrinkage, highlighted by a widespread porosity, likely due to the quenching process. In both samples, the average size of crystals is very small (below 30 μm) and only the analyses on *Mix_00_C1.5* showed a Cl content in aluminate phases, C_4AF and in a microcrystalline Cl-rich phase, irregular in shape (Fig. 12) and with the average composition reported as last analysis in Table 3, that may be identified as $Ca_{12}Al_{14}O_{32}[\square_4Cl_2]$, chlormayenite [35].

5. Discussion

For the sake of clarity, the discussion will be split into two sections: in the former, the effects of magnesium, sulphur, and sodium in coupled presence will be introduced and compared with the literature data; in the latter, the effects of chlorine addition in the already Na_2O-SO_3-MgO doped mixtures will be discussed.

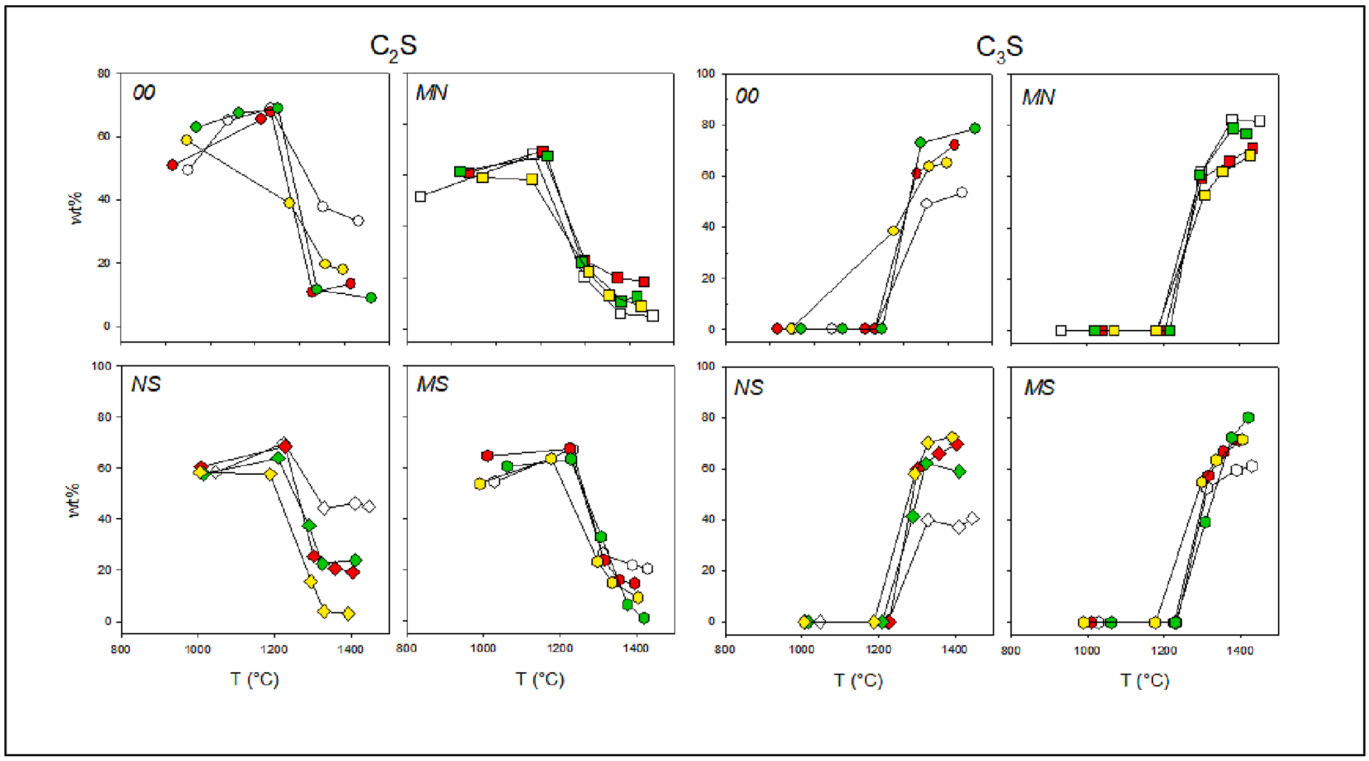

Fig. 4. Rietveld quantitative phase analysis results for C_2S and C_3S for all in-situ mixtures: empty white, red, green and yellow symbols refer to 0%, 0.5%, 1.0% and 1.5% $CaCl_2$ doping, respectively; symbol size is always larger than esd (3σ). (For interpretation of the references to colour in this figure legend, the reader is referred to the web version of this article.)

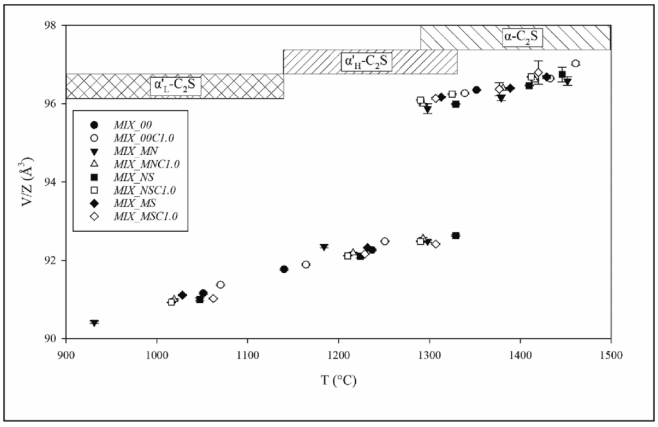

Fig. 5. V/Z (Å^3) of C_2S vs temperature on heating for in-situ SXRPD experiments with 1 wt% $CaCl_2$ and no chlorine doping; 3σ is reported as error bars for each analysis.

5.1. *MgO-Na_2O-SO_3 doped Portland cement clinker*

The combination of MgO and SO_3 remarkably affects the raw meal's behavior upon clinkering, in such a way that a strong correlation between species is suggested. *In-situ* experiments highlight that the dopants mainly influence the 2nd stage of heating (temperature higher than 1350 °C). Magnesium has a predominant effect during sintering, boosting the C_3S formation through the reaction CaO + α-C_2S → R-C_3S, despite the occurrence of sulphur, which is expected to promote the C_2S stabilization even at higher temperature [36,37]. Furthermore, at high-temperature the occurrence of an immiscible sulphur-rich liquid phase in coexistence with a Fe-Al silicate is commonly mentioned in presence of S^{4+} [38–40]. However, microstructural investigation did not highlight sulphate melt phase evidence in our experiments despite the occurrence of alkali sulphate (i.e., aphitalite). We suppose that the sulphur solubility in the Fe-Al silicate liquid phase is favored by high-temperature, leading to a general decrease of its viscosity and promoting the C_3S growth. Magnesium and sulphur compete for the polymorph stabilization of C_3S during clinkering. Mg^{2+} preferably stabilizes M_3-C_3S by the ionic substitution $Mg^{2+} \rightarrow Ca^{2+}$ reducing its cell volume (Å^3) [11,20,33,41–47], whereas sulphur stabilizes M_1-C_3S through the ionic substitution $2^{IV}Al^{3+} + {}^{IV}S^{6+} \rightarrow 3^{IV}Si^{4+}$ that promotes an increase of cell volume [21,43,44]. On the other hand, the overall cell volume reductions observed during clinkering for both C_3S polymorphs in comparison with their pure counterparts suggest that: (i) Mg^{2+} can be a species involved in ionic replacements in the M_1-C_3S crystal structure and not only in the M_3 polymorph as expected; (ii) the Mg-ionic exchange has a stronger effect on the volume reduction than the above-described ionic substitution (i.e., $2^{IV}Al^{3+} + {}^{IV}S^{6+} \rightarrow 3^{IV}Si^{4+}$). The incorporation of Mg^{2+} and S^{6+} in the calcium silicate crystal structures is also confirmed by chemical analyses by EMPA (Table 3). The simultaneous occurrence of Mg^{2+} and S^{6+} tends to stabilize the intermediate temperature β-C_2S phase [36,37,48,49], exploiting the same ionic substitutions previously reported for C_3S. In doped samples, the larger volume cell of β-C_2S than that of the reference pure phase [36] is explained by the incorporation of S^{6+} and Al^{3+} in place of Si^{4+}. Upon cooling, minor elements presumably redistribute among the clinker phases leading to higher contents of M_1-C_3S. On the other hand, the observed decrease of C_3A and increase of C_4AF suggest that the dopants promote the stability field of C_4AF at the expanse of C_3A in the CaO-Al_2O_3-Fe_2O_3-SiO_2 system [36,49,50]. This is in keeping with the C_4AF increase in the final doped clinker, thus causing a decrease of available Al_2O_3 from the liquid phase, detrimental to C_3A crystallization. Therefore, magnesium and sulfur simultaneous occurrence at the explored content does not negatively affect PC properties (i.e., overall C_3S and C_2S contents), or even improves the control of orthorhombic celite formation, allowing the possible reuse of Mg- and S-rich materials (i.e.,

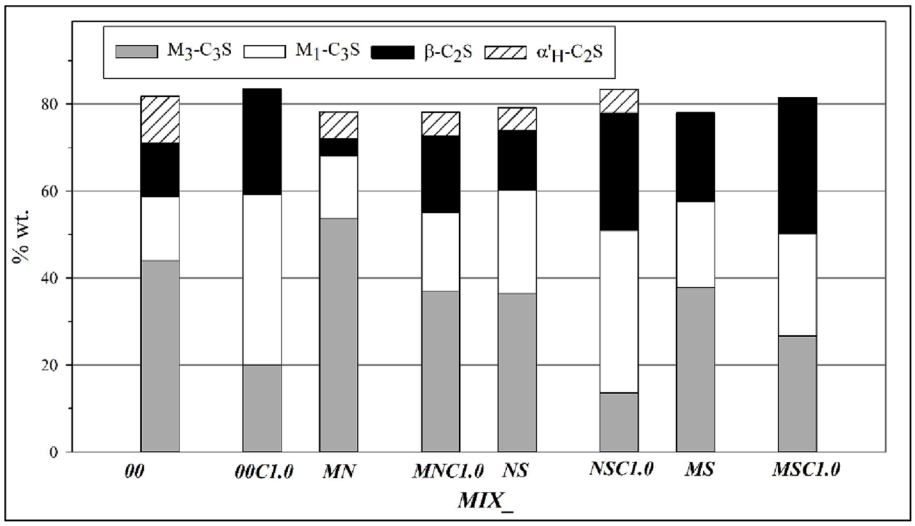

Fig 6. Ex-situ LXRPD Rietveld results (wt.%) for silicate crystal phases.

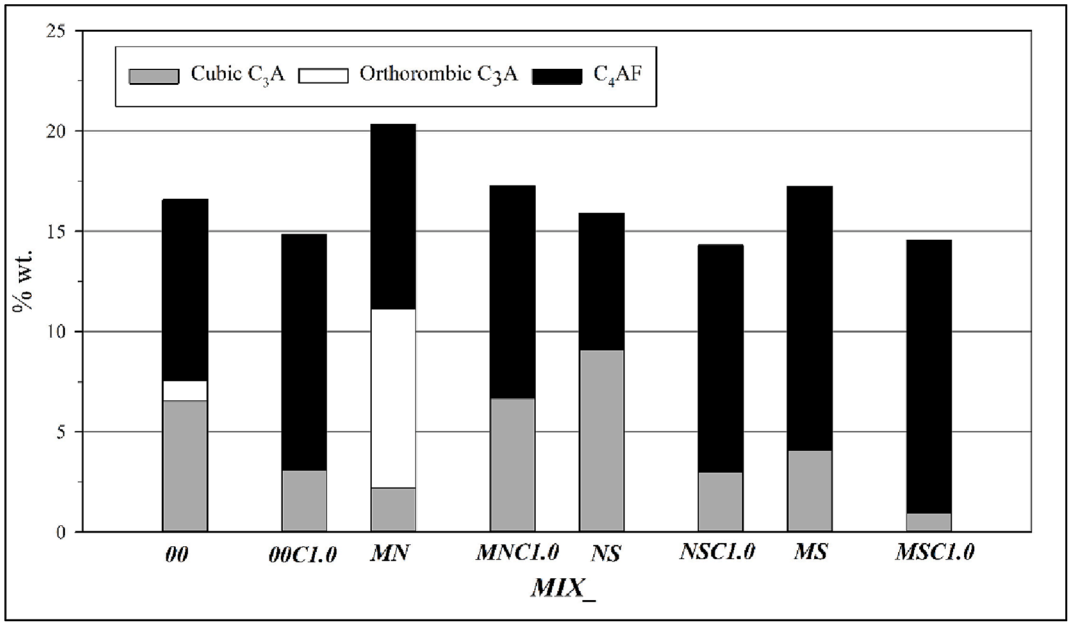

Fig. 7. Ex-situ LX RPD Rietveld results (wt.%) for aluminate crystal phases.

impure limestone and wastes).

During the 1st stage of clinkering the presence of magnesium and sodium favors the formation of α'_H-C_2S by the ionic substitutions involving sodium, calcium and cation vacancies $2Na^+ \rightarrow Ca^{2+} + \square$ during solid state reactions [36,49,50]. At higher temperature, the Na-doped α-C_2S, reported as highly reactive belite clinker [8], transforms with lime leading to the formation of R-C_3S. Note that R-C_3S stabilization is also boosted by magnesium occurrence, whose abundance reaches 75 wt% at 1450 °C. During cooling, the dopants leave the high-temperature silicate clinker phases (R-C_3S and α-C_2S) and (i) redistribute through the aluminate phases, thus affecting their final content, and (ii) promote the crystallization of accessory phases. In particular, sodium partly abandons R-C_3S because of its lesser solubility in the C_3S structure [36] than in the liquid phase. This results in the stabilization of the orthorhombic C_3A driven by the ionic exchange $Na^+ + Si^{4+} \rightarrow Ca^{2+} + Al^{3+}$ [26,47,51,52]. Moreover, the excess of Na_2O not hosted by the main clinker phases is incorporated in accessory phases, such as aphthitalite and/or thenardite [36,49,50]. Due to the absence of SO_3, magnesium preferably enters the C_3S crystal structure promoting M_3-C_3S stabilization in large quantities (see Table 1S), as indicated by the cell volume decrease. The slight increase in amount of α'_H-C_2S confirms the role of Na^+ in the stabilization of this high-temperature polymorph, increasing the vacancies content and cell volume [53]. Therefore, Na_2O and MgO simultaneous doping could be used in cement manufacture (i) to boost the formation of C_3S at lower temperatures and (ii) to promote high-temperature dicalcium silicate polymorphs. However, the main drawback is the preferred stabilization of orthorhombic celite, which worsen the control of setting during hydration [36,49].

The combination of sulphur and sodium leads to the stabilization of higher contents of C_2S during the 1st stage of clinkering and confirms the role of sulphur on the belite stabilization. On the other hand, we cannot exclude that also sodium promotes the C_2S growth by entering the C_2S structure through ionic substitutions involving vacancies $2Na^+ \rightarrow Ca^{2+} + \square$ or $2Na^+ + \square \rightarrow 2Ca^+ + O^{2-}$. At higher temperature the two dopants do not increase the liquid phase amount as expected from literature. Rather they both act as mineralizers for C_2S, thus slowing the rate of

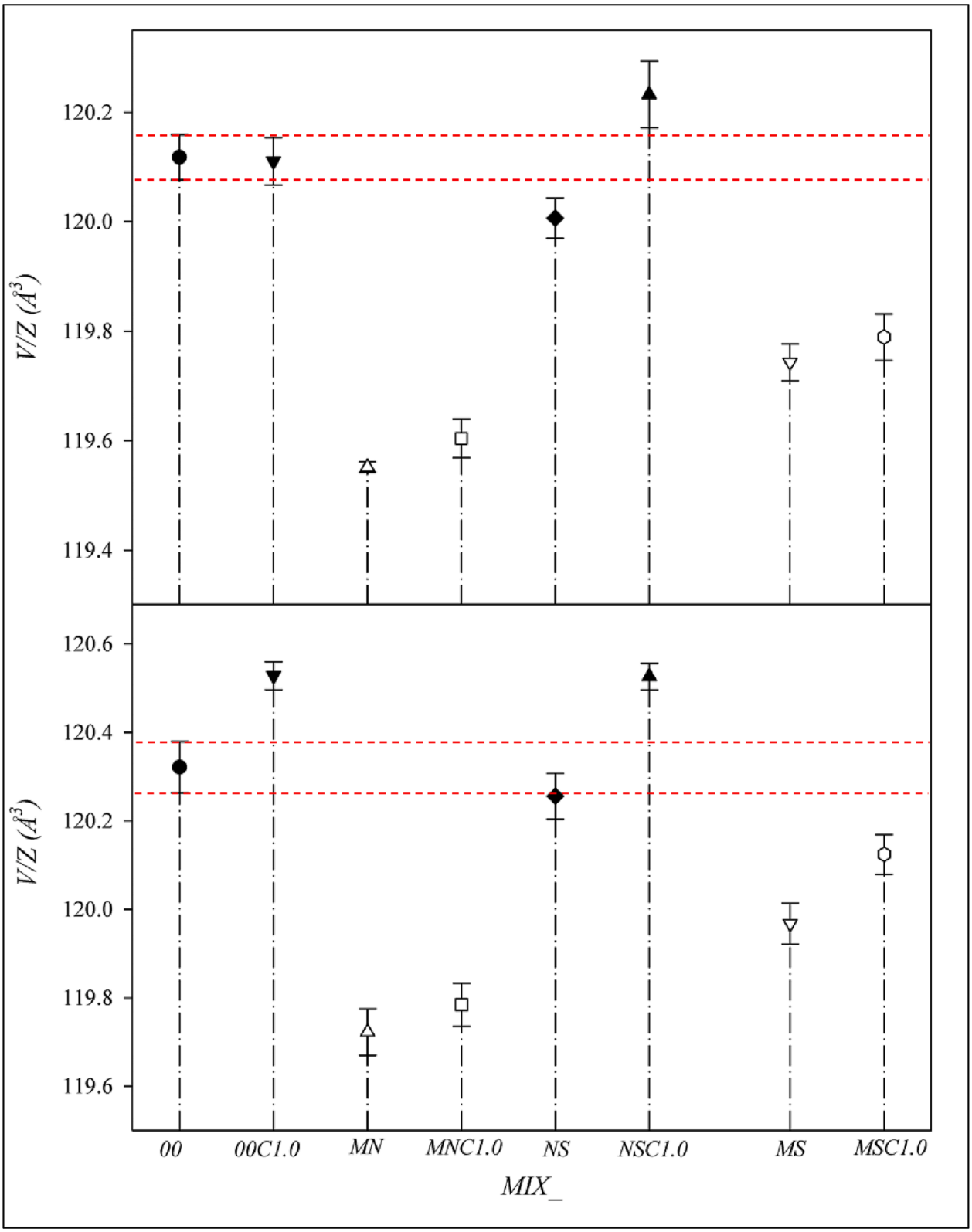

Fig. 8. Normalized volume (volume of formula unit, V/Z, Å^3) for (a) M_3-C_3S and (b) M_1-C_3S for ex-situ LXRPD samples; horizontal red dashed lines represent the ± 3σ of MIX_00; 3σ is reported as error bars for each analysis. (For interpretation of the references to colour in this figure legend, the reader is referred to the web version of this article.)

alite formation and resulting in an increase of free CaO in the system (Table 2, Fig. 2). During cooling, the doping with sodium and sulphur affects the proportions of the polymorphs in clinker, mainly through the M_1-C_3S, β-C_2S and cubic C_3A stabilization at room temperature. This behavior is likely explained by the stronger efficacy of sulphur in stabilizing β-C_2S and cubic C_3A than sodium in promoting α'$_H$-C_2S and orthorhombic C_3A. The very low capacity of clinker phases to host sodium results in a Na-enrichment of the liquid phase, which favors

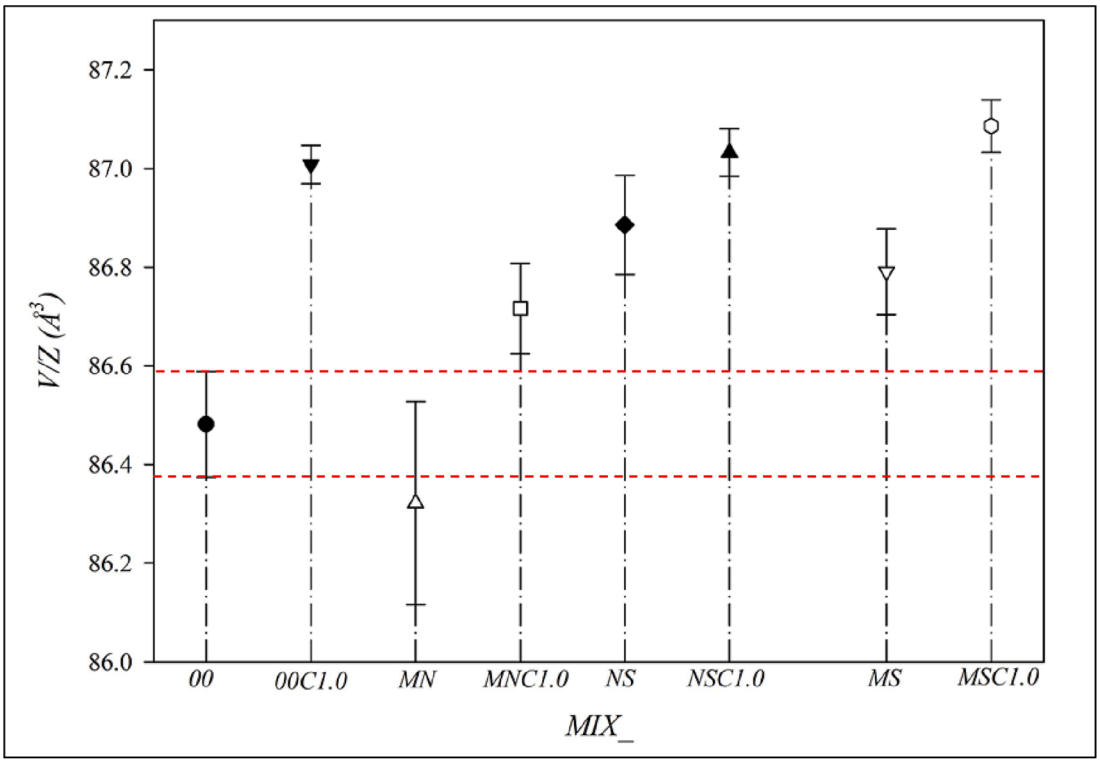

Fig. 9. Normalized volume (volume for unit formula, V/Z, Å^3) for β-C_2S for ex-situ LXRPD samples; 3σ is reported as error bars for each analysis.

crystallization of aphthitalite as major sodium-rich crystal phase at room temperature [36,49,50]. However, the simultaneous doping with Na_2O and SO_3 does not negatively affect the overall crystal phases composition of PC as revealed by *ex-situ* results, pointing out positive reuse of impure natural materials and wastes as alternative raw materials.

5.2. Na_2O-MgO-SO_3-Cl doped Portland cement clinker

In the present study the *in-situ* HT-SXRPD experiments allow us to clarify the clinkering mechanisms that occur upon heating in Cl-doped samples and help explain the mineralogical composition and microstructure of the final PC. Note that the effects induced by Cl *via* $CaCl_2$ dominate upon those due to the other species involved; therefore, for the sake of simplicity we chose to focus on the Na_2O-MgO-SO_3-Cl system, rather than to investigate the individual couples Na_2O-Cl, MgO-Cl and SO_3-Cl. In the 1st stage of heating, the reaction between quartz and a Cl-rich liquid phase produced by $CaCO_3$-$CaCl_2$ melting at 630 °C gives $Ca_3SiO_4Cl_2$ [49]. At higher temperature, $CaCO_3$ progressively decomposes into CaO + CO_2 and the free lime reacts with quartz producing C_2S, as expected from literature [36,49,50]. In Table 2 the similar contents of C_2S in the samples with Cl at 0.5 and 1 wt% suggest that chlorine does not catalyze C_2S formation. Between 750 and 900 °C the crystallization of the aluminate occurs, and chlorine promotes the crystallization of $C_{12}A_7$ at the expense of C_3A, especially for high Cl contents. This results in a very low content of C_3A in the final clinker in comparison with standard PC (see discussion below). EMPA data confirm that $C_{12}A_7$ preferentially hosts chlorine through the ionic substitution $Cl^- + Si^{4+} \rightarrow O^{2-} + Al^{3+}$ [35]. Furthermore, small quantities of chlorine are seen also in C_4AF crystals, thus proving that Cl-ion substitutions occur in the ferrite structure. At $T > 1000$ °C, $Ca_3SiO_4Cl_2$ decomposes into C_2S and CaO through a solid-state reaction. No occurrence of alinite ($Ca_{11}Si_4O_{16}Cl$) is observed, confirming that its formation requires higher contents of chlorine in the starting meal [54–61]. At higher temperature (~1300 °C), a liquid phase appears from the dissolution of the aluminates. The higher content of the liquid phase reported in Table 2 hints that also $C_{12}A_7$ melts. The chlorine ions released from chlormayenite are not incorporated into a preferred crystal phase, rather they induce complexation leading to a decrease of the liquid phase viscosity upon heating [49]. In this light, chlorine can be likened to a flux promoting ion diffusion and thus speeding up the C_3S formation without affecting its final content [36,49,50]. Furthermore, the lack of chlorine in the silicate crystals (Table 3) confirms that it behaves as a modifier of the liquid phase's physical properties, rather than being incorporated into silicate crystal phases. Therefore, the increase in the cell volume values observed for all the calcium silicate phases (Fig. 8, Fig. 9) is mainly attributable to the incorporation of sodium, magnesium and sulphur into their crystal structures. *Ex-situ* results reveal that chlorine affects the relative proportions of polymorphs: it increases the stability of M_1-C_3S, save for magnesium-rich samples where high contents of the M_3 polymorph are seen. Chlorine inhibits the orthorhombic C_3A growth and overall celite formation, even in the Na-doped samples, in contrast with expectations. Furthermore, Cl-doping reduces and increases the overall alite and belite contents, respectively, excepted in the absence of other dopants (i.e., *MIX_00*). Cl does not significantly promote the growth of C_4AF. The microstructure of the final doped-PC clinkers is very similar to the one observed in the standard PC [36]. In particular, the addition of chlorine to the doped mixture influences neither the crystal grain size nor the phase composition [62]. Recalculation of the chlorine content from EMPA (i.e., ~ 0.04 wt% vs 1.15 wt% are the calculated and the original content respectively) shows a partial depletion in Cl. This can be attributed to the fact that chlorine is volatile and a fraction evaporates from Cl-rich phases during the heat-treatment process, resulting in a non-uniform chlorine distribution in the final products.

Therefore, the addition of chlorine in already Na-Mg-S-doped raw meals affects:

(i) Physical-chemical properties of the liquid phase upon heating, leading lower viscosity, improving wettability and increasing the Ca-silicate crystal rate of growth;

Table 3
Chemical composition (wt.%) of the main clinker phases detected by EMPA analyses; esd (1σ) is reported in rounded brackets.

*MIX_*	*00C1.0*	*MNC1.0*	*NSC1.0*	*MSC1.0*	*MNC1.5*	*00C1.0*	*MNC1.0*	*NSC1.0*	*MSC1.0*	*00C1.5*	*MNC1.5*	*00C1.0*	*NSC1.0*	*MSC1.0*	*00C1.5*	*MNC1.5*	*MNC1.5*	*00C1.5*
Phase	**C_3S**(16 pts.)	**C_3S**(5 pts.)	**C_3S**(16 pts.)	**C_3S**(16 pts.)	**C_3S**(2 pts.)	**C_2S**(16 pts.)	**C_2S**(5 pts.)	**C_2S**(15 pts.)	**C_2S**(15 pts.)	**C_2S**(3 pts.)	**C_2S**(3 pts.)	**C_4AF**(5 pts.)	**C_4AF**(8 pts.)	**C_4AF**(8 pts.)	**C_4AF**(2 pts.)	**C_4AF**(4 pts.)	**C_3A**(3 pts.)	**$C_{12}A_7$**(6 pts.)
SiO_2	24.32 (0.41)	24.61 (0.34)	24.68 (0.33)	24.58 (0.37)	23.23 (1.66)	29.66 (0.43)	29.21 (0.78)	29.34 (0.93)	29.30 (0.45)	33.05 (0.14)	28.47 (0.30)	5.63 (1.63)	3.89 (0.28)	5.41 (0.15)	8.22 (1.48)	2.16 (0.76)	2.79 (0.26)	4.36 (1.52)
TiO_2	0.16(5)	0.17(4)	0.15(8)	0.11(5)	0.24(6)	0.26(9)	0.28(4)	0.24(6)	0.26(4)	0.14(9)	0.30(3)	0.71 (0.19)	1.12 (0.16)	0.91 (0.21)	1.45 (0.56)	0.99 (0.28)	0.02(2)	0.07(3)
Al_2O_3	1.18 (0.37)	1.22 (0.50)	1.09 (0.15)	1.07 (0.19)	3.24 (1.13)	2.04 (0.15)	1.84 (0.30)	2.08 (0.21)	2.20 (0.14)	0.62 (0.54)	2.42 (0.19)	20.15 (2.38)	19.50 (1.40)	19.66 (1.29)	14.15 (1.14)	21.81 (2.19)	30.26 (0.52)	35.76 (2.75)
Fe_2O_3	0.75 (0.30)	0.76 (0.34)	0.70 (0.10)	0.58 (0.13)	2.23 (0.18)	1.24 (0.16)	0.95 (0.14)	1.31 (0.11)	1.15(8)	0.25 (0.17)	1.42(5)	17.27	20.28 (1.73)	15.43 (1.19)	25.42 (1.56)	21.85 (1.55)	4.32 (0.33)	4.40 (0.54)
MnO	0.06(4)	0.06(5)	0.06(3)	0.05(3)	0.15 (0.18)	0.08(3)	0.07(3)	0.06(2)	0.06(2)	0.01(2)	0.06(5)	0.58 (0.23)	1.10 (0.25)	0.66 (0.27)	1.16 (0.18)	1.02 (0.29)	0.03(2)	0.03(1)
MgO	0.81(4)	1.50(7)	0.81(5)	1.51(6)	0.96 (0.19)	0.37 (0.20)	0.71 (0.31)	0.42 (0.17)	0.57 (0.26)	0.03(1)	0.39(8)	2.68 (0.40)	3.01 (0.61)	4.71 (0.30)	1.38 (0.25)	2.35 (0.28)	0.67 (0.25)	0.57 (0.51)
CaO	71.54 (0.63)	69.78 (1.38)	72.26 (0.51)	71.83 (0.43)	68.50 (0.85)	63.71 (0.77)	63.14 (0.67)	63.40 (0.94)	63.43 (0.68)	63.68 (0.52)	63.42 (0.69)	51.10 (2.39)	48.65 (0.63)	50.03 (0.28)	49.63 (1.01)	48.04 (0.52)	60.25 (0.54)	48.01 (1.86)
Na_2O	0.02(2)	0.15(6)	0.10(4)	0.01(1)	0.05(3)	0.03(2)	0.57 (0.19)	0.47(8)	0.03(2)	n.d	0.18(4)	0.02(1)	0.21 (0.10)	0.03(1)	0.01(1)	0.02(1)	0.13(2)	0.01(1)
K_2O	n.d.	n.d.	0.01(1)	n.d.	n.d.	n.d.	0.08	0.10	n.d.	n.d.	0.02(1)	n.d.	0.07(2)	0.01(1)	n.d.	n.d.	n.d.	0.01(1)
SrO	0.11(8)	0.14(7)	0.15 (0.11)	0.13 (0.14)	0.17 (0.15)	0.30 (0.11)	0.33 (0.16)	0.30 (0.10)	0.34(8)	0.28(8)	0.25 (0.11)	0.16(8)	0.24(9)	0.16 (0.14)	0.14(7)	0.08(3)	0.16(9)	0.14(9)
SO_3	0.12(5)	0.16(9)	0.20(5)	0.19(4)	0.29(8)	0.83 (0.15)	0.78 (0.21)	1.42 (0.28)	1.42 (0.16)	0.37 (0.35)	1.60 (0.14)	0.34 (0.12)	0.85 (0.10)	1.20 (0.36)	0.18(5)	0.09(9)	0.02(1)	0.12(5)
F	0.01(2)	0.01(2)	n.d.	n.d.	n.d.	n.d.	n.d.	n.d.	n.d.	n.d.	n.d.	0.01(1)	n.d.	n.d.	n.d.	n.d.	n.d.	n.d.
Cl	0.01(1)	0.01(1)	0.01(1)	0.01(1)	0.03(1)	0.01(1)	n.d.	0.01(1)	0.01(1)	0.01(1)	0.02(1)	0.07(1)	0.01(1)	0.11(3)	0.22(5)	0.02(1)	0.01(1)	3.83 (0.39)
O = F + Cl	0.01	0.01	n.d.	n.d.	0.01	n.d.	n.d.	n.d.	n.d.	n.d.	0.01	0.02	n.d.	0.03	0.05	n.d.	n.d.	0.86
Total	99.09 (0.76)	98.59 (0.24)	100.21 (0.49)	100.07 (0.46)	99.05 (0.55)	98.52 (1.04)	97.96 (0.41)	99.15 (1.14)	98.78 (1.29)	98.44 (0.86)	98.55 (0.95)	98.71 (1.27)	98.90 (1.17)	98.31 (1.07)	101.93 (1.26)	98.40 (1.47)	98.66 (0.86)	96.40 (1.12)
Si	0.935	0.943	0.946	0.934	0.888	0.875	0.861	0.859	0.857	0.965	0.838	0.221	0.154	0.211	0.318	0.086	0.129	1.103
Ti	0.005	0.005	0.004	0.003	0.007	0.006	0.006	0.005	0.006	0.003	0.007	0.021	0.033	0.026	0.042	0.030	0.001	0.012
Al	0.053	0.049	0.051	0.048	0.146	0.071	0.090	0.072	0.076	0.021	0.084	0.931	0.907	0.902	0.645	1.027	1.648	10.668
Fe	0.022	0.019	0.021	0.016	0.064	0.028	0.026	0.029	0.025	0.006	0.032	0.509	0.603	0.452	0.740	0.657	0.150	0.931
Mn	0.002	0.002	0.002	0.002	0.005	0.002	0.002	0.002	0.002	–	0.002	0.019	0.037	0.022	0.038	0.034	0.001	0.001
Mg	0.046	0.087	0.044	0.086	0.054	0.016	0.037	0.018	0.024	0.001	0.017	0.156	0.177	0.273	0.080	0.140	0.046	0.0.213
Ca	2.946	2.894	2.913	2.923	2.806	2.013	1.975	1.989	1.998	1.992	2.001	2.145	2.058	2.087	2.058	2.057	2.983	13.020
Na	0.001	0.010	0.009	0.001	0.004	0.002	0.036	0.027	0.002	–	0.010	0.001	0.016	0.002	–	0.001	0.011	0.006
K	–	–	0.001	–	–	–	0.003	0.004	–	–	0.001	–	0.003	–	–	–	–	0.002
Sr	0.002	0.003	0.004	0.003	0.004	0.005	0.006	0.005	0.006	0.005	0.004	0.004	0.005	0.004	0.003	0.002	0.004	0.021
S	0.004	0.004	0.008	0.006	0.008	0.018	0.018	0.031	0.031	0.008	0.035	0.010	0.025	0.035	0.005	0.003	0.001	0.023
F	0.002	0.001	–	–	–	–	–	–	–	–	–	0.001	–	–	–	–	–	–
Cl	–	0.001	–	–	0.002	–	–	–	–	–	0.001	0.005	–	0.007	0.014	0.001	0.001	1.641
Σ	4.02	4.02	4.00	4.02	3.98	3.03	3.06	3.04	3.02	2.99	3.03	4.02	4.02	4.02	3.93	4.03	4.97	25.98

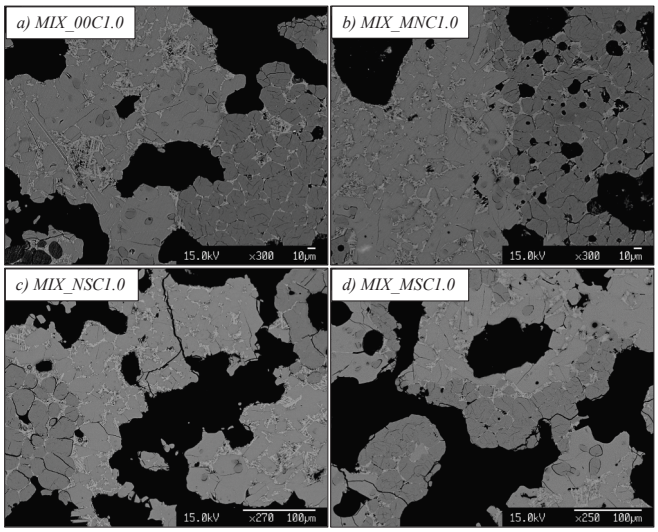

Fig. 10. BSE images from SEM analysis highlighting microstructural features of 1% $CaCl_2$ doped clinker.

(ii) Polymorph phases proportions upon cooling stabilizing M_1-C_3S, cubic C_3A and β-C_2S;
(iii) The appearance of Cl-rich phases, such as chlormayenite, when Cl content is higher than 1.0 wt%;
(iv) Alite content that tends to reduce only when simultaneously occurs with other dopants;
(v) Alkali sulphate crystallisation (i.e. aphthitalite) which is inhibited in the case of Cl-doping even with sodium and sulphur doping;
(vi) Celite content which reduces even with high sodium content.

5.3. General considerations

Our outcomes highlighted that minor element effects should be used to improve cement manufacture (i.e., enhancing PC properties and reducing energy consumption and CO_2 emission) and circular economy development (i.e., waste reuses, reduction of quarried raw materials). Despite the reuse of wastes (e.g., mine tailing, phosphogypum, fly ash, bottom ash, among others) and impure natural raw materials (e.g., dolomite-rich limestone, impure limestone, volcanic ashes and impure clays) to the starting raw meal being a fundamental objective for today's society, they do not only increase individual minor elements content but also add a plethora of dopants that can even negatively influence cement qualities. Moreover, each alternative raw material has a different chemical variability, especially in the case of impure natural materials, and can also change during time (i.e., chemical composition changes inside limestone/clay quarry, changes related to different chemical treatments for wastes). Therefore, it is essential to detailly evaluate the effect of each individual doping element and multiple element occurrence, even at difference concentration, for properly reusing impure materials; otherwise, negatively effects (i.e., degradation of cement properties) can not be predicted and debatably handled. On this way this study aimed to clarify effects of common minor elements occurring in impure materials, giving special attention on chlorine effects both alone and in combination with other elements: *ex-situ* analysis helped in reproducing similar PC manufacture especially for revealing minor element effects on microstructure; whereas *in-situ* experiments showed the effects at different temperatures of minor elements during heating on phase assemblage and melt formation.

MgO, Na_2O and SO_3 represent most common minor elements of several alternative raw materials, whose effects, as coupled dopant elements, were broadly evaluated in this study. The simultaneous occurrence of all these three dopants should not lead strong changes on overall alite and belite contents, but likely an increase in celite content negatively affecting setting during hydration. Therefore, basing on the results of Cl-free mixtures, a possible solution capable of (*a*) both including MgO, Na_2O and SO_3 in PC raw meal and (*b*) simultaneously improving PC properties, or at least maintaining similar features, should be to add phosphorous as further minor element:

(i) to increase final monoclinic C_3S is strictly needed to increase high-temperature polymorphs of dicalcium silicate (i.e., α'_H- C_2S and α-C_2S) during 1st and 2nd stages so final boosting R-C_3S. Na_2O is able to improve high-temperature dicalcium silicate polymorphs, especially during 1st stage, but R-C_3S formation is limited in the case of SO_3 doping. Nonetheless, MgO addition should limit SO_3 negative effects on C_3S formation. However, P_2O_5 doping with low amount (<1 wt% [49,63]) is able to lower dicalcium silicate polymorphic transition, especially if coupled with Na_2O, thanks to the ionic substitutions ($Na^+ + {}^{IV}P^{5+} \rightarrow Ca^{2+} + {}^{IV}Si^{4+}$ or $2\,{}^{IV}P^{5+} + \rightarrow 2\,{}^{IV}Si^{4+} + Ca^{2+}$ [49]), boosting R-C_3S crystallization even at lower temperature [7];

(ii) to reduce the overall content of C_3A and preferably stabilize cubic polymorph, P_2O_5 doping is needed due to strong influence of Na_2O occurrence. Na_2O is able to both increase celite content and mainly stabilize orthorhombic polymorph, excepted when is coupled with sulphur which only celite content increased. However, P_2O_5 addition

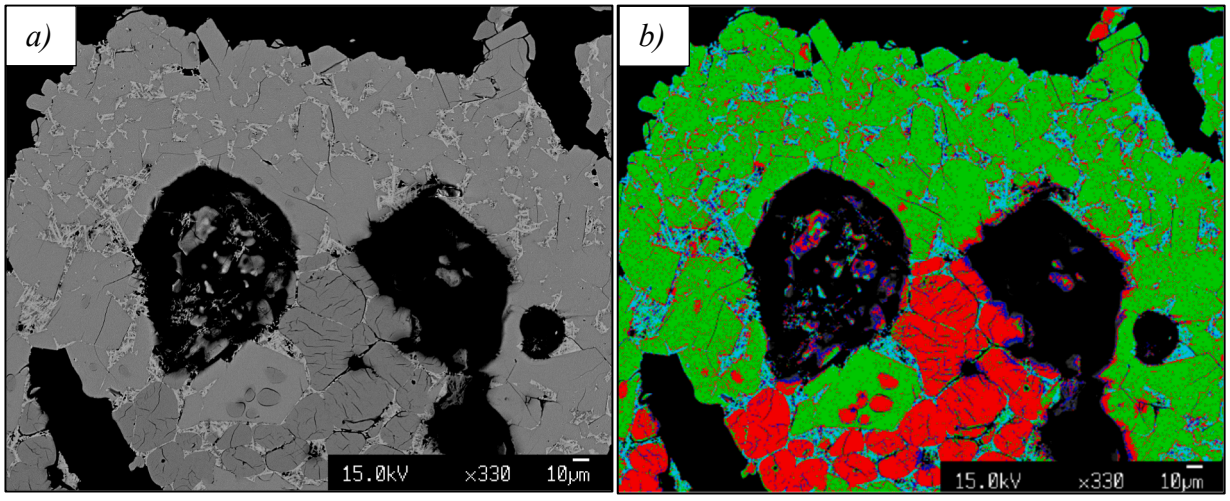

Fig. 11. (a) BSE image from SEM analysis of MIX_00C1.0, and (b) its colour segmentation reporting in cyan C_4AF, green C_3S, red C_2S and sky blue C_3A. (For interpretation of the references to colour in this figure legend, the reader is referred to the web version of this article.)

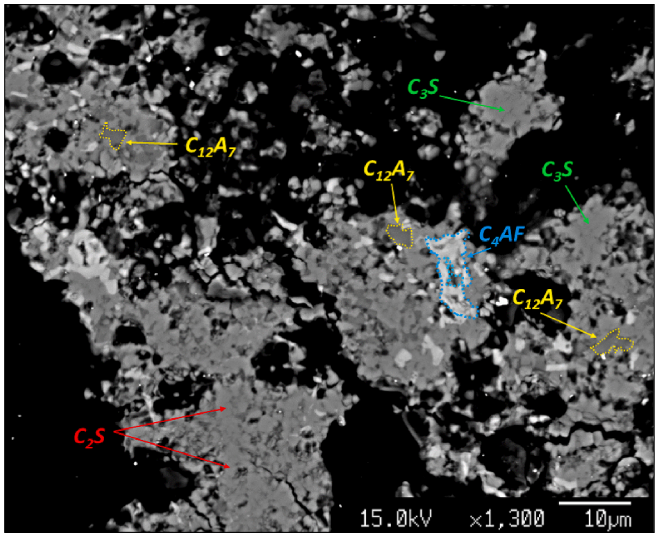

Fig. 12. BSE image of sample MIX_00C1.5; yellow circles mark the position of Cl-rich $C_{12}A_7$. (For interpretation of the references to colour in this figure legend, the reader is referred to the web version of this article.)

along with MgO, SO_3 and Na_2O, should lead lower C_3A content thanks to higher content of high-temperature dicalcium silicate polymorphs which are able to host most Na^+ and P^{5+} resulting in a Na-depleted melt, limiting negative Na_2O effects.

Furthermore, considerations should be made on the use of Cl-doping in PC manufacture: Cl addition has positive effects on (*a*) lowering melt viscosity (i.e., promoting ionic diffusion and R-C_3S formation), (*b*) inhibiting alkali sulphate crystallization during cooling (i.e., aphthitalite formation), (*c*) strong reducing celite content and (*d*) inhibiting orthorhombic celite formation; whereas, negative effects are mostly related to lower and higher alite and belite contents, respectively, excepted in the case of Cl-doping in pure PC raw meal. Therefore, Cl-doping should be limited in the case of simultaneous occurrence of other dopants, conversely a deterioration of PC properties occurs; whereas, free-doped PC raw meal should not exceed 0.7 wt%, otherwise rings inside kiln will form [64].

Chlorine is found in two main wastes that could be used in cement manufacture as alternative raw materials acting as Cl-doping sources: (i) Municipal Solid Waste Incineration (MSWI, also known as bottom and fly ashes) produced from burning urban solid wastes that could partially replace raw mixture, carrying several minor element P_2O_5, Na_2O, K_2O, TiO_2, SO_3 and Cl) [65]; (ii) Chlorinated Hydrocarbons (CHs) representing liquid wastes which could be mixed with the fuel and usually add only Cl to the heated raw meal [64]. Both MSWI and CHs represent environmental endangering wastes which have to be properly treated (i.e., chemically treated, incapsulated and stocked in special disposal) [66], otherwise environmental pollution can easily occur. Therefore, considering the treatment costs, potential pollutants release and disposal soil consumption, MSWI and CHs should be both used in cement manufacture as alternative raw materials.

Afterwards, considering all this evidence, cement manufacture has revealed the clear potential to properly treat a wide range of wastes as alternative raw materials producing PC with similar or even better properties, and improving Circular Economy. However, more experiments should be made with a gradual increase in the number of dopants simulating "natural" recycling condition. By doing so, a comprehensive understanding of main minor element effects will be achieved enabling us to design doped raw mixtures both mitigating potential negative effects and properly reusing several waste materials.

6. Conclusions

The effects of chlorine ($CaCl_2$) alone or in combination with other common minor elements, such as magnesium, sodium and sulphur, on Portland Cement phases (their microstructural features, proportions and chemical composition) were explored in detail by both *in-situ* and *ex-situ* investigation. *In-situ* and *ex-situ* experiments allowed us to observe the effects induced by different chlorine contents in cement raw meals upon heating and on cooling, respectively. Moreover, the correlations between minor elements were proven to impact foremost onto the polymorph phases occurrence and secondly onto the relative amount of C_3S and C_2S.

Chlorine influences the clinker phases independently of the other dopants here explored, leading to three main effects: (i) chlorine tends to lower and increase alite and belite, respectively, especially at high content, excepted in absence of other dopants which leads opposite effect; (ii) chlorine increases the stability field of mayenite ($C_{12}A_7$) during heating, at the expense of celite (C_3A) that melts in the clinkering zone ($T \sim 1350$ °C) and releases Cl-ions in the melt, thus lowering viscosity and wettability, which thing promotes Ca-silicate formation; (iii) chlorine strongly influences polymorph phases, preferably stabilizing M_1-C_3S, β-C_2S and cubic C_3A; (iv) chlorine is mostly volatized during heating, remaining trapped inside cement kiln, and partly hosted in $C_{12}A_7$. No changes in the microstructural features and total amount of the Ca-silicate phases ($C_3S + C_2S$) are observed with respect to standard PC clinkers.

Declaration of Competing Interest

The authors declare the following financial interests/personal relationships which may be considered as potential competing interests: Nicoletta Marinoni reports financial support was provided by Government of Italy Ministry of Education University and Research (MIUR; Project PRIN2017-2017L83S77).

Data availability

Data will be made available on request.

Acknowledgments

The authors acknowledge the support of the Italian Ministry of Education. The authors would like to thank A. Risplendente, who performed SEM and EMPA analysis and AG. De la Torre for her support in the revision of the text. This research was funded by the Italian Ministry for Education, University and Research (MIUR; project PRIN2017-2017L83S77).

Appendix A. Supplementary data

Supplementary data to this article can be found online at https://doi.org/10.1016/j.conbuildmat.2023.132261.

References

[1] F.S. Bourgeois, N.R. Lippiatt, M.S. Powell, Introducing the concept of mechanical texture in comminution: The case of concrete recycling, Int. J. Miner. Process. 136 (2015) 7–14.
[2] G. Bernardo, M. Marroccoli, M. Nobili, A. Telesca, G.L. Valenti, The use of oil well-derived drilling waste and electric arc furnace slag as alternative raw materials in clinker production, Resour. Conserv. Recycl. 52 (1) (2007) 95–102.
[3] P.E. Tsakiridis, G.D. Papadimitriou, S. Tsivilis, C. Koroneos, Utilization of steel slag for Portland cement clinker production, J. Hazard. Mater. 152 (2) (2008) 805–811.
[4] Q. Wu, Y. Wu, W. Tong, H. Ma, Utilization of nickel slag as raw material in the production of Portland cement for road construction, Constr. Build. Mater. 193 (2018) 426–434.
[5] M. Segata, N. Marinoni, M. Galimberti, M. Marchi, M. Cantaluppi, A. Pavese, Á. G. De la Torre, The effects of MgO, Na2O and SO3 on industrial clinkering process:

phase composition, polymorphism, microstructure and hydration, using a multidisciplinary approach, Mater. Charact. 155 (2019) 109809.
[6] T.R. Jensen, A.N. Christensen, J.C. Hanson, Hydrothermal transformation of the calcium aluminum oxide hydrates CaAl2O4·10H2O and Ca2Al 2O5·8H2O to Ca3Al 2(OH)12 investigated by in situ synchrotron X-ray powder diffraction, Cem. Concr. Res. 35 (12) (2005) 2300–2309.
[7] Á.G. De la Torre, K. Morsli, M. Zahir, M.A.G. Aranda, In situ synchrotron powder diffraction study of active belite clinkers, J. Appl. Crystallogr. 40 (6) (2007) 999–1007.
[8] Á.G. De La Torre, A.J.M. Cuberos, G. Álvarez-Pinazo, A. Cuesta, M.A.G. Aranda, In situ powder diffraction study of belite sulfoaluminate clinkering, J. Synchrotron Radiat. (2011), https://doi.org/10.1107/S0909049511005796.
[9] S. Gerassimidou, C.A. Velis, P.T. Williams, M.J. Castaldi, L. Black, D. Komilis, Chlorine in waste-derived solid recovered fuel (SRF), co-combusted in cement kilns: A systematic review of sources, reactions, fate and implications, Crit. Rev. Environ. Sci. Technol. 51 (2) (2021) 140–186.
[10] M. Simoni, T. Hanein, T.Y. Duvallet, R.B. Jewell, J.L. Provis, H. Kinoshita, Producing cement clinker assemblages in the system: CaO-SiO2-Al2O3-SO3-CaCl2-MgO, Cem. Concr. Res. 144 (2021) 106418.
[11] Á.G. De la Torre, R.N. De Vera, A.J.M. Cuberos, M.A.G. Aranda, Crystal structure of low magnesium-content alite: Application to Rietveld quantitative phase analysis, Cem. Concr. Res. 38 (11) (2008) 1261–1269.
[12] J. Rydberg, Wavelength dispersive X-ray fluorescence spectroscopy as a fast, non-destructive and cost-effective analytical method for determining the geochemical composition of small loose-powder sediment samples, J. Paleolimnol. 52 (3) (2014) 265–276.
[13] J.-L. Hodeau, P. Bordet, M. Anne, A. Prat, A.N. Fitch, E. Dooryhee, G. Vaughan, A. K. Freund, Nine-crystal multianalyzer stage for high-resolution powder diffraction between 6 keV and 40 keV, Cryst. Multilayer Opt. (1998), https://doi.org/10.1117/12.332525.
[14] A.N.F. Jon, P. Wright, G.B.M. Vaughan, Merging data from a multi-detector continuous scanning powder diffraction system, Eur. Synchrotron Radiat. Facil. (2003). https://www.iucr.org/resources/commissions/crystallographic-computing/newsletters/1/merging-data.
[15] S.M. Moussa, R.M. Ibberson, M. Bieringer, A.N. Fitch, M.J. Rosseinsky, In situ measurement of cation order and domain growth in an electroceramic, Chem. Mater. 15 (13) (2003) 2527–2533.
[16] J.W. Edwards, R. Speiser, H.L. Johnston, High temperature structure and thermal expansion of some metals as determined by x-ray diffraction data. I. Platinum, tantalum, niobium, and molybdenum, J. Appl. Phys. 22 (4) (1951) 424–428.
[17] B.H. Toby, R.B. Von Dreele, GSAS-II: The genesis of a modern open-source all purpose crystallography software package, J. Appl. Crystallogr. 46 (2) (2013) 544–549.
[18] M. Cantaluppi, N. Marinoni, F. Cella, A. Bravo, F. Cámara, G. Borghini, W. Kagan, An insight on the effect of sodium and silicon on microstructure and crystallography of high alumina cements, Cem. Concr. Res. 148 (2021), 106533, https://doi.org/10.1016/J.CEMCONRES.2021.106533.
[19] M. Cantaluppi, F. Cámara, The crystal structure of Na2CaAl4O8 and its hydration behaviour, J. Solid State Chem. 303 (2021) 122478.
[20] Á.G. De La Torre, S. Bruque, J. Campo, M.A.G. Aranda, The superstructure of C3S from synchrotron and neutron powder diffraction and its role in quantitative phase analyses, Cem. Concr. Res. 32 (9) (2002) 1347–1356.
[21] M.-N. de Noirfontaine, F. Dunstetter, M. Courtial, G. Gasecki, M. Signes-Frehel, Polymorphism of tricalcium silicate, the major compound of Portland cement clinker: 2. Modelling alite for Rietveld analysis, an industrial challenge, Cem. Concr. Res. 36 (1) (2006) 54–64.
[22] F. Dunstetter, M.-N. de Noirfontaine, M. Courtial, Polymorphism of tricalcium silicate, the major compound of Portland cement clinker, Cem. Concr. Res. 36 (1) (2006) 39–53.
[23] W.G. Mumme, R.J. Hill, G. Bushnell-Wye, E.R. Segnit, Rietveld crystal structure refinements, crystal chemistry and calculated powder diffraction data for the polymorphs of dicalcium silicate and related phases, Neues Jahrb. Fuer Mineral. (1995).
[24] K.H. Jost, B. Ziemer, R. Seydel, Redetermination of the structure of β-dicalcium silicate, Acta Crystallogr. Sect. B Struct. Crystallogr. Cryst. Chem. 33 (6) (1977) 1696–1700.
[25] P. Mondal, J.W. Jeffery, The crystal structure of tricalcium aluminate, Ca 3 Al 2 O 6, Acta Crystallogr. Sect. B Struct. Crystallogr. Cryst. Chem. 31 (3) (1975) 689–697.
[26] F. Nishi, Y. Takéuchi, The A1 6 O 18 rings of tetrahedra in the structure of Ca 8.5 NaAl 6 O 18, Acta Crystallogr. Sect. B Struct. Crystallogr. Cryst. Chem. 31 (4) (1975) 1169–1173.
[27] G.J. Redhammer, G. Tippelt, G. Roth, G. Amthauer, Structural variations in the brownmillerite series Ca2(Fe2-xAlx)O5: Single-crystal X-ray diffraction at 25 °C and high-temperature X-ray powder diffraction (25 °C ≤ T ≤ 1000 °C), Am. Mineral. 89 (2-3) (2004) 405–420.
[28] G. Fiquet, P. Richet, G. Montagnac, High-temperature thermal expansion of lime, periclase, corundum and spinel, Phys. Chem. Miner. 27 (2) (1999) 103–111.
[29] J. Zhang, Effect of pressure on the thermal expansion of MgO up to 8.2 GPa, Phys. Chem. Miner. 27 (3) (2000) 145–148.
[30] K. Kihara, An X-ray study of the temperature dependence of the quartz structure, Eur. J. Mineral. 2 (1) (1990) 63–78.
[31] T. Sakakura, K. Tanaka, Y. Takenaka, S. Matsuishi, H. Hosono, S. Kishimoto, Determination of the local structure of a cage with an oxygen ion in Ca12Al14O33, Acta Crystallogr. Sect. B Struct. Sci. 67 (3) (2011) 193–204.
[32] K. Okada, J. Ossaka, Structures of potassium sodium sulphate and tripotassium sodium disulphate, Acta Crystallogr. Sect. B Struct. Crystallogr. Cryst. Chem. 36 (4) (1980) 919–921.
[33] F. Nishi, Y. Takéuchi, The rhombohedral structure of tricalcium silicate at 1200 °C, Zeitschrift Fur Krist. - New Cryst. Struct. 168 (1-4) (1984) 197–212.
[34] L. Glasser, H.D.B. Jenkins, Lattice energies and unit cell volumes of complex ionic solids, J. Am. Chem. Soc. 122 (4) (2000) 632–638.
[35] E.V. Galuskin, I.O. Galuskina, J. Kusz, F. Gfeller, T. Armbruster, R. Bailau, M. Dulski, V.M. Gazeev, N.N. Pertsev, A.E. Zadov, P. Dzierżanowski, Mayenite supergroup, part II: Chlorkyuygenite from Upper Chegem, Northern Caucasus, Kabardino-Balkaria, Russia, a new microporous mineral with “zeolitic” H2O, Eur. J. Mineral. 27 (1) (2015) 113–122.
[36] H.F.W. Taylor, Cement chemistry, 2nd ed., Acad. Press, 1997.
[37] Cement Chemistry by H. F. Taylor, J. Coast. Res. 15 (2012).
[38] Y.B. Pliego-Cuervo, F.P. Glasser, Role of sulphates in cement clinkering: The calcium silicosulphate phase, Cem. Concr. Res. 8 (4) (1978) 455–459.
[39] Y.B. Pliego-Cuervo, F.P. Glasser, The role of sulphates in cement clinkering: Subsolidus phase relations in the system CaO-A℄2O3-SiO2-SO3, Cem. Concr. Res. 9 (1) (1979) 51–55.
[40] T.W. W., No Title, 7th Int. Conf. Cem. Concr. 1 (1980) 1–3.
[41] M. Bigare, A. Guinier, C. Mazieres, M. Regourd, N. Yannaquis, W. Eysbl, T.H. Hahn, E. Woermann, Polymorphism of tricalcium silicate and its solid solutions, J. Am. Ceram. Soc. 50 (11) (1967) 609–619.
[42] M. Courtial, M.-N. de Noirfontaine, F. Dunstetter, G. Gasecki, M. Signes-Frehel, Polymorphism of tricalcium silicate in Portland cement: A fast visual identification of structure and superstructure, Powder Diffr. 18 (1) (2003) 7–15.
[43] F. Dunstetter, M.-N. de Noirfontaine, M. Courtial, Polymorphism of tricalcium silicate, the major compound of Portland cement clinker: 1. Structural data: Review and unified analysis, Cem. Concr. Res. 36 (1) (2006) 39–53.
[44] M.-N. de Noirfontaine, M. Courtial, F. Dunstetter, G. Gasecki, M. Signes-Frehel, Tricalcium silicate Ca3SiO5 superstructure analysis: A route towards the structure of the M1 polymorph, Zeitschrift Fur Krist. 227 (2) (2012) 102–112.
[45] J.W. Jeffery, The crystal structure of tricalcium silicate, Acta Crystallogr. 5 (1) (1952) 26–35.
[46] F. Nishi, Y. Takeuchi, I. Maki, Tricalcium silicate Ca30[Si04]: The monoclinic superstructure, Zeitschrift Fur Krist. - New Cryst. Struct. (1985), https://doi.org/10.1524/zkri.1985.172.3-4.297.
[47] D. Stephan, S. Wistuba, Influence of the inclusion of foreign ions on the structure, reactivity and hydration products of tricalcium silicate and tricalcium aluminate, Cem. Int. (2005).
[48] P.C. Hewlett, M. Liska, Lea’s chemistry of cement and concrete, 2019. https://doi.org/10.1016/C2013-0-19325-7.
[49] W. Kurdowski, Cement and concrete chemistry, 2014. https://doi.org/10.1007/978-94-007-7945-7.
[50] P.C. Hewlett, Lea’s Chemistry of Cement and Concrete, 2003. https://doi.org/10.1016/B978-0-7506-6256-7.X5007-3.
[51] F.C. Lee, H.M. Banda, F.P. Glasser, Substitution of Na, Fe and Si in tricalcium aluminate and the polymorphism of solid solutions, Cem. Concr. Res. 12 (2) (1982) 237–246.
[52] G.Y. Shin, F.P. Glasser, Interdependence of sodium and potassium substitution in tricalcium aluminate, Cem. Concr. Res. 13 (1) (1983) 135–140.
[53] K. Fukuda, H. Taguchi, T. Fukuda, Effect of substituent ions on martensitic transformation temperatures in dicalcium silicate solid solutions, J. Am. Ceram. Soc. 85 (7) (2002) 1804–1806.
[54] F.v. Lampe, W. Hilmer, K.H. Jost, G. Reck, A.I. Boikova, Synthesis, structure and thermal decomposition of alinite, Cem. Concr. Res. 16 (4) (1986) 505–510.
[55] J. Neubauer, H. Pöllmann, Alinite - Chemical composition, solid solution and hydration behaviour, Cem. Concr. Res. 24 (8) (1994) 1413–1422.
[56] Y.-M. Kim, S.-H. Hong, H. Kim, Synthesis and hydration characteristics of Alinite cement, J. Am. Ceram. Soc. 85 (8) (2002) 1941–1946.
[57] D. Mowla, A. Jahanmiri, H.R. Fallahi, Preparation and optimization of alinite cement in various temperatures and CaCl2 content, Chem. Eng. Commun. 171 (1) (1999) 1–13.
[58] M. Singh, P.C. Kapur, Pradip, Pradip, Preparation of alinite based cement from incinerator ash, Waste Manag. 28 (8) (2008) 1310–1316.
[59] H. Shi, K. Wu, K. Deng, F. Yuan, Preparation of alinite cement clinker from municipal solid waste incinerator fly ash, Kuei Suan Jen Hsueh Pao/J. Chin. Ceram. Soc. (2009).
[60] G.O. Uçal, M. Mahyar, M. Tokyay, Hydration of alinite cement produced from soda waste sludge, Constr. Build. Mater. 164 (2018) 178–184.
[61] G.O. Uçal, M. Mahyar, M. Tokyay, I. Yaman, Low-Energy Alinite Cement From Soda Sludge Waste, Am. Concr. Institute, ACI Spec. Publ., 2017.
[62] D.H. Campbell, Microscopical Examination and Interpretation of Portland Cement and Clinker, 1999.
[63] S. Boughanmi, I. Labidi, A. Megriche, H. Tiss, A. Nonat, Does phosphorus affect the industrial Portland cement reactivity? Constr. Build. Mater. 188 (2018) 599–606.
[64] B. Ahling, Destruction of chlorinated hydrocarbons in a cement kiln, Environ. Sci. Technol. 13 (11) (1979) 1377–1379.
[65] N. Saikia, S. Kato, T. Kojima, Production of cement clinkers from municipal solid waste incineration (MSWI) fly ash, Waste Manag. 27 (9) (2007) 1178–1189.
[66] R. Kikuchi, Recycling of municipal solid waste for cement production: Pilot-scale test for transforming incineration ash of solid waste into cement clinker, Resour. Conserv. Recycl. 31 (2) (2001) 137–147.